Counting near-infrared single-photons with 95% efficiency

Adriana E. Lita,[1,*] Aaron J. Miller,[2] and Sae Woo Nam[1]

[1]*National Institute of Standards and Technology, 325 Broadway, Boulder CO 80305, USA*
[2]*Department of Physics, Albion College, Albion MI 49224, USA*
**Corresponding author: lita@boulder.nist.gov*

Abstract: Single-photon detectors operating at visible and near-infrared wavelengths with high detection efficiency and low noise are a requirement for many quantum-information applications. Superconducting transition-edge sensors (TESs) are capable of detecting visible and near-infrared light at the single-photon level and are capable of discriminating between one- and two-photon absorption events; however these capabilities place stringent design requirements on the TES heat capacity, thermometry, and optical detection efficiency. We describe the fabrication and evaluation of a fiber-coupled, photon-number-resolving TES detector optimized for absorption at 1550 and 1310 nm wavelengths. The measured system detection efficiency at 1556 nm is 95 % ± 2 %, which to our knowledge is the highest system detection efficiency reported for a near-infrared single-photon detector.

OCIS codes: (220.0220) Optical design and fabrication; (270.5570) Quantum Detectors

References and links

1. A. L. Migdal, D. Branning, and S. Castelletto, "Tailoring single-photon and multiphoton probabilities of a single-photon on-demand source," Phys. Rev. A **66,** 053805 (2002).
2. D. Bouwmeester, "Quantum physics – high noon for photons," Nature **429,** 139-141 (2004).
3. E. Knill, R. Laflamme, and G. J. Milburn, "A scheme for efficient quantum computation with linear optics," Nature **409,** 46-52 (2001).
4. P. A. Hiskett D. Rosenberg, C. G. Peterson, R. J. Hughes, S. Nam, A. E. Lita, A. J. Miller and J. E. Nordholt, "Long distance quantum key distribution in optical fibre," New J. Phys. **8**, 193 (2006).
5. A. K. Ekert, "Quantum cryptography based on Bell's theorem, " Phys. Rev. Lett. **67**, 661-663 (1991), C.H. Bennett, G. Brassard, and N. D. Mermin, "Quantum cryptography without Bell's theorem," Phys. Rev. Lett. **68**, 557-559 (1992).
6. D. C. Burnham and D. L. Weinberg, "Observation of Simultaneity in Parametric Production of Optical Photon Pairs," Phys. Rev. Lett. **25**, 84-87 (1970).
7. D. Rosenberg, S. Nam, A. J. Miller, A. Salminen, E. Grossman, R. E. Schwall, and J. M. Martinis, "Near-unity absorption of near-infrared light in tungsten films," Nucl. Instrum. Methods Phys. Res. A **520**, 537-540, (2004).
8. B. Cabrera, R. M. Clarke, P. Colling, A. J. Miller, S. Nam, and R. W. Romani, "Detection of single infrared, optical, and ultraviolet photons using superconducting transition edge sensors," Appl. Phys. Lett. **73**, 735-737 (1998).
9. A. J. Miller, S. Nam, J. M. Martinis and A. V. Sergienko, "Demonstration of a low-noise near-infrared photon counter with multiphoton discrimination," Appl. Phys. Lett., **83**, 791-793 (2003).
10. D. Rosenberg, A. E. Lita, A. J. Miller and S. Nam, "Noise-free high-efficiency photon-number-resolving detectors," Phys Rev. A **71**, 061803 (2005).
11. A. E. Lita, D. Rosenberg, S. Nam, A. J. Miller, D. Balzar, L. M. Kaatz, and R. E. Schwall, "Tuning of tungsten thin film superconducting transition temperature for fabrication of photon number resolving detectors," IEEE Trans. Appl. Supercond. **15**, 3528-3531 (2005).
12. R. Ohba, I. Uehira and S. Kakuma, "Interferometric determination of a static optical path difference using a frequency swept laser diode," Meas. Sci. Technol. **1**, 500-504 (1990).
13. K. D. Irwin, "An application of electrothermal feedback for high resolution cryogenic particle detection," Appl. Phys. Lett. **66**, 1998-2000 (1995).

#91219 - $15.00 USD Received 2 Jan 2008; revised 14 Feb 2008; accepted 16 Feb 2008; published 20 Feb 2008

14. M. E. Huber, A. M. Corey, K. L. Lumpkins, F. N. Nafe, J. O. Rantschler, G. C. Hilton, J. M. Martinis, and A. H. Steinbach, "DC SQUID series arrays with intracoil damping to reduce resonance distortions," Applied Superconductivity **5**, 425 (1998)
15. J. N. Ullom, W. B. Doriese, G. C. Hilton, J. A. Beall, S. Deiker, W. D. Duncan, L. Ferreira, K. D. Irwin, C. D. Reintsema, and L. R. Vale, "Characterization and reduction of unexplained noise in superconducting transition-edge sensors, "Appl. Phys. Lett. **84**, 4206-4208 (2004).
16. A. J. Miller, A. E. Lita, D. Rosenberg, S. Gruber, S. Nam, "Superconducting photon number resolving detectors: performance and promise," Proceedings of the 8th International Conference on Quantum Communication, Measurement and Computing, J. O. Hirota, H. Shapiro and M. Sasaki, Eds., NICT Press, 445-450, (2007).

1. Introduction

Single-photon detectors with high quantum efficiency, photon-number-resolving capabilities and very low dark-count rate are mandatory to enable a number of applications in the field of quantum information such as photon source and detector calibration [1], *n*-photon state quantum optics experiments [2], photon-based quantum computing [3] and long-distance quantum key distribution (QKD) [4]. In particular, linear optics quantum computing and quantum cryptography [5] require the controlled generation of single photons and of multiphoton entangled states. Spontaneous parametric down-conversion (PDC) [6] is presently the best source for heralded single-photon states, in which two strongly time-correlated photons are emitted each into one of two spatial modes, and the detection of a photon in one of the spatial modes indicates with high probability the presence of the pair photon in the other spatial mode. For such heralded single-photon states, conventional detectors that are unable to distinguish between one or two photons may be used. However, in order to achieve heralding of an entangled multiphoton state, all of the photons involved in the multiphoton protocol must be measured to ensure the creation of the desired heralded multiphoton state. In this case, detectors that have high efficiency and have the ability to unambiguously resolve photon number are required. Superconducting transition-edge sensors (TESs), with tungsten as the active device material, are microcalorimeters that have photon-number resolution with negligible dark counts. The devices described in this paper can be optimized for high quantum efficiency at particular wavelengths from near-ultraviolet to near-infrared by designing multilayer device structures that include integrated thin-film layers that enhance the absorption of light into the active device material [7].

A general microcalorimeter device consists of an absorber for the incident energy, a thermometer to measure the temperature increase resulting from the absorption of energy, and a weak thermal link that enables the cooling of the absorber to its base temperature once the measurement of device temperature is complete. TESs for visible and near-infrared wavelengths have been fabricated from tungsten (W) because of the tunability of its superconducting transition temperature (T_c) in the ~ 100 mK range and the relative weak coupling between its electron and phonon systems at these temperatures [8]. Detection of visible and near-infrared light at single-photon levels requires stringent control of the device heat capacity and sensitive absorber thermometry. In our W TESs, the electron subsystem in the thin film of W acts as both the absorber and the thermometer. The anomalously low thermal coupling between the electrons and phonons in W provides a weak thermal link from the electron system to the phonon system at base temperature. The steep change in resistance vs. temperature at the superconducting critical temperature results in a very sensitive measure of temperature, enabling precise measurements of the energy of single photons.

In this paper we report our record system detection efficiency of 95 % for a single-photon detector at 1556 nm including all system losses.

2. Device fabrication

The detection efficiency of a system using a bare tungsten TES detector (with no optical cavity structure) was measured to be 20 % at near-infrared wavelengths [9]. The main

#91219 - $15.00 USD Received 2 Jan 2008; revised 14 Feb 2008; accepted 16 Feb 2008; published 20 Feb 2008

sources of loss were fiber-to-detector alignment, reflection from the surface of the W film, and transmission of light through the thin W film. Previously, by embedding the W TES in an optical structure designed to enhance absorption, and by improving the coupling efficiency of optical fibers to the devices, we achieved a system detection efficiency of ~ 89 % at 1550 nm [10]. Using the same principles, we designed and fabricated an optical structure that maximizes absorption at both major telecommunication wavelengths: 1550 and 1310 nm. Fig. 1 shows the absorption curves in large-area tungsten films extracted from reflectivity measurements. The curves shown correspond to a W film embedded in an optimized optical structure as well as a bare tungsten film, both measured at room temperature. By embedding the tungsten film in the optical structure the absorption was increased at almost one hundred percent from absorption of bare tungsten at both 1310 nm and 1550 nm wavelengths.

The W absorbers used in the TESs described in this paper measure 25x25 μm^2 and are approximately 20 nm thick with T_c=178 ±5 mK. These sensors have superconducting transition temperature higher than those for the previous generation, which enables thermal recovery times to be less than 1 μs while maintaining excellent number discrimination between multiphoton events.

We have calculated the index of refraction for all cavity layers using the reflectance and transmittance data collected with a spectrophotometer. Using the indices of refraction for the layers in a thin-film modeling program, we have designed the structure (layer thicknesses) that simultaneously enhances absorption in tungsten at 1310 and 1550 nm wavelengths. In our optical cavity design we use a trilayer structure rather than the bare tungsten film. The trilayer amorphous-Si/W/amorphous-Si is deposited *in situ*, which was found to enhance and stabilize the tungsten T_c against thermal-stress-induced suppression. These stresses arise from the differences in coefficients of thermal expansion of the various dielectric and metallic layers used in the design [11].

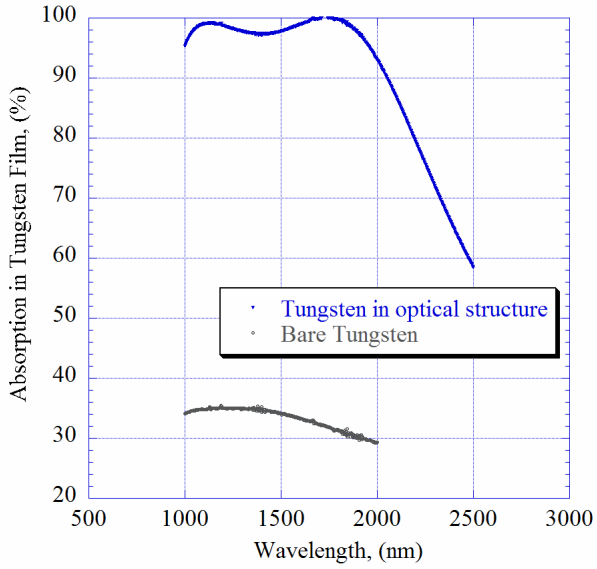

Fig. 1. (Color online) Spectrophotometer data taken at room temperature indicating significant improvement in tungsten absorption at both 1310 and 1550 nm wavelengths when tungsten is embedded between appropriate dielectric layers.

The optical structure is designed to maximize photon absorption in the W layer. Beginning from the side of the device farthest from the incident light, this structure consists of a back-side reflecting mirror (electron-beam evaporated Al film ~80 nm thick), a dielectric spacer (physical vapor deposition (PVD) grown layer of SiO2 ~220 nm thick, plus a layer of DC-

#91219 - $15.00 USD Received 2 Jan 2008; revised 14 Feb 2008; accepted 16 Feb 2008; published 20 Feb 2008

sputtered amorphous-Si (a-Si) ~16 nm thick), followed by the W detector layer (DC-sputtered high-purity W, 20 nm thick). Finally, an antireflecting (AR) coating is deposited on top of the W detection layer (DC-sputtered a-Si ~ 62 nm plus a PVD-grown layer of SiO2 ~ 160 nm thick). Measurements of the structure reflectivity indicate that the expected intrinsic device efficiency, neglecting system losses, is greater than 98 % at both 1550 nm and 1310 nm wavelengths (Fig. 1).

3. Device packaging/alignment

Coupling and alignment losses typically reduce the measured efficiency of the detector, known as system detection efficiency, from the expected device efficiency (in our case greater than 98 %). Photons are coupled to the detector through a standard 9 μm core single-mode, telecommunication fiber. The exit end of the fiber (i.e., the end closest to the device) has an antireflective coating for 1550 nm that reduces the fraction of light reflected back up the fiber from ~ 4 % to less than ~ 1 %. The fiber is aligned under a microscope at room temperature using back-side through-chip imaging. Once the fiber is centered above the detector, the housing holding the fiber is clamped to the detector housing. This complete detector package is subsequently operated at a temperature less than 100 mK using an adiabatic demagnetization refrigerator.

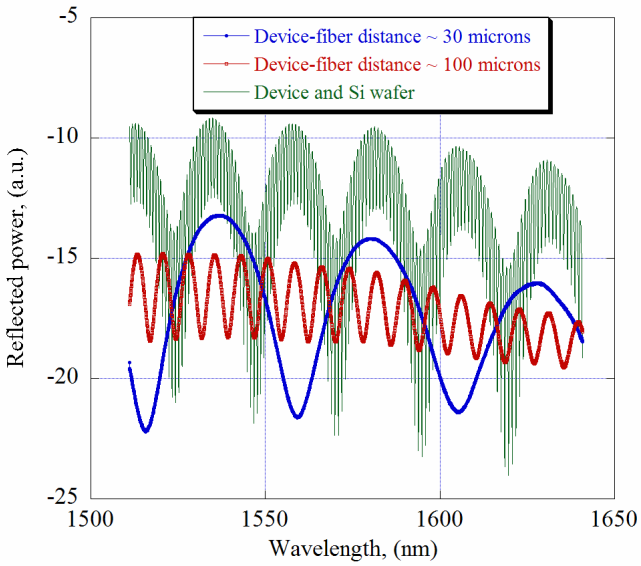

Fig. 2. (Color online) Interference patterns corresponding to different fiber-to-detector distances and also illustrating the small Δλ fringes in the case when light is incident on the device but also Si substrate, because of lateral misalignment.

To assess the fiber-to-detector spacing at both room temperature and cryogenic temperatures we implement a method originating from swept-frequency laser interferometry [12]. Using a tunable laser, circulator, and power meter, we sweep the laser wavelength and observe resulting periodic fringes in the back-reflected power. These fringes result from interference between the ~ 1% reflection of exit end of the fiber and the residual light reflected from the surface of the detector. The spacing of the fringes allows us to determine the static optical path difference between the fiber and the device; this path difference is simply two times the fiber-to-detector distance and, therefore, the distance from fiber to detector d can be estimated as $d \cong \lambda^2/2\Delta\lambda$, where λ is the average wavelength over the scan and Δλ is the fringe spacing. Using this method and knowing how much d shrinks due to thermal contraction of

#91219 - $15.00 USD Received 2 Jan 2008; revised 14 Feb 2008; accepted 16 Feb 2008; published 20 Feb 2008

detector package, we can position the fiber to within 10 μm of the device surface when at cryogenic temperatures.

Upon cooling to cryogenic temperatures, the detector package undergoes thermal contraction that could result in lateral misalignment between the fiber and the small device, causing light to hit the substrate near the device instead of being absorbed in the W. Using the swept-frequency interferometry we can crudely assess the amount of incident light that is not incident on the detector. If light hits areas around the detector, it can propagate through the Si wafer and reflect off the polished back-side. This optical path is significantly longer than the fiber-to-device path (the Si substrate is > 200 μm thick whereas the fiber-to-device path is ~10 μm). This long path introduces interference fringes with small $\Delta\lambda$ that are superimposed on the fringe pattern resulting from light hitting only the device (Fig. 2). This is an important tool to confirm that alignment of the fiber to the detector is preserved after cooling to cryogenic temperatures.

4. Device performance

4.1 Measurement setup

The TES device produces an electrical signal that is proportional to the temperature increase of the absorber resulting from the absorption of a photon. The absorber temperature is measured by an ultrasensitive thermometer consisting of a tungsten thin film that is voltage biased within its superconducting-to-normal transition (T_c ~178 mK). The stability of the voltage bias is due to negative electro-thermal feedback (ETF) [13]. When a photon is absorbed, it produces a photoelectron that heats up the tungsten electron system. This heat in excess of the quiescent Joule heating at equilibrium is removed through negative ETF in the form of a drop in the Joule power dissipation. Consequently, the optical energy deposited in the absorber (W electron system) can be calculated by multiplying the time integral of the change in current (ΔI) by the bias voltage ($V_{\rm bias}$) : $E=V_{\rm bias}\int\Delta I(t)dt$.

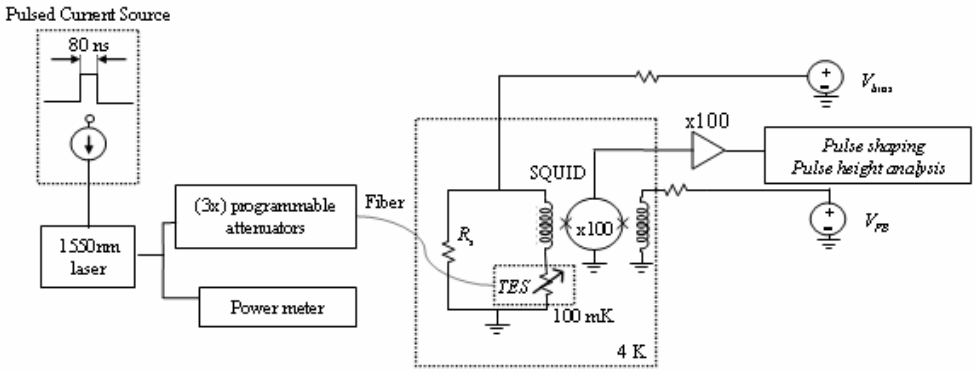

Fig. 3. Schematic of the optical and electrical measurement circuit.

The schematic of our measurement setup is shown in Fig. 3. The light source is a pulsed 1550 nm laser, heavily attenuated through three programmable attenuators and fiber-coupled to a single-mode fiber. The fiber-aligned detector package is mounted to the base stage of a cryogen-free adiabatic demagnetization refrigerator and cooled down to subKelvin temperatures. The detector voltage bias is provided by a stable room-temperature current source (I_{bias}) shunted through a small resistor (R_s ~ 20 mΩ) at 4 K, in parallel with the TES. The detector current is amplified by a low-noise cryogenic preamp consisting of a 100-element series array of dc-superconducting quantum interference device (SQUID) amplifiers [14] at 4 K. The sensor current induces a flux through the SQUID via the input coil. The

#91219 - $15.00 USD Received 2 Jan 2008; revised 14 Feb 2008; accepted 16 Feb 2008; published 20 Feb 2008

resulting voltage signal is further amplified and filtered using room-temperature electronics that performs pulse shaping and pulse height analysis.

4.2 I-V Characteristics

The device electrical characteristics are displayed in Fig. 4. The superconducting transition temperature is 178 ±5 mK.

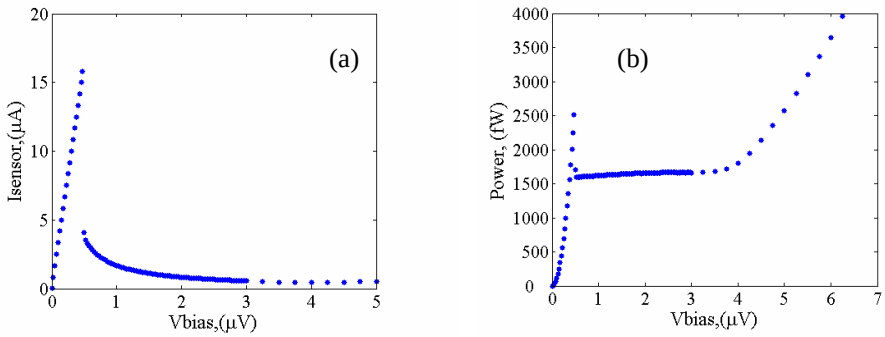

Fig. 4. Current (a) and power (b) as a function of voltage bias, respectively. Below 3 μV the sensor is self-biased, and the power is approximately constant as a function of voltage. Device base temperature is ~ 72 mK.

The power dissipated by the TES device in the self-biased region (where the power is constant with the applied voltage), is known as the quiescent power. The TES is operated as a single-photon detector in the self-biased region. Any heat (from photon absorption) in excess of the quiescent Joule heating at equilibrium is removed by negative ETF: the increase in the electron temperature in tungsten raises the resistance and results in a drop of the Joule power dissipated. The energy absorbed by the tungsten can then be calculated by integrating the corresponding drop in current multiplied by the bias voltage.

4.3 Device energy resolution

Using the measured quiescent power and known device geometry and material parameters, we can estimate the expected energy resolution. Following the calculation in [8], the W electronic heat capacity is given by $C = \gamma T$ with $\gamma = 1.3$ mJ/(mole-K^2) and is then multiplied by 2.43, the factor from the Bardeen-Cooper-Schrieffer (BCS) theory, corresponding to the increase in heat capacity of a superconductor just below T_c. We obtain $C = 0.74$ fJ/K for our detector volume of 25 μm x 25 μm x 20 nm. From Fig. 4(b) we extract the quiescent power as $P_0 = 1600$ fW. For substrate temperatures well below T_c we can estimate the thermal conductances using the formula $g = dP/dT \sim nP_0/T_c$, where n is the power law dependence of the thermal conductance between the electron system and the substrate ($n = 5$ for electron-phonon limited conductance [8]). We obtain a thermal conductance $g = 56$ pW/K for our system. Consequently, the intrinsic time constant $\tau_0 = C/g$, is 13 μs. The actual time constants we measure are smaller due to ETF and relate to the intrinsic time constants through $\tau_{ETF} = \tau_0/(1+\alpha/n)$, where $\alpha = d\ln R / d\ln T\big|_{V=\text{constant}}$ and describes the sharpness of the superconducting transition [13]. The measured time constant is typically ~ 800 ns, giving $\alpha \sim$ 60. The theoretical energy resolution limit is given by

$$\Delta E_{FWHM} = 2.355\sqrt{4k_B T_c^2 C\left(\frac{1}{\alpha}\right)\sqrt{\left(\frac{n}{2}\right)}} \qquad (1)$$

#91219 - $15.00 USD Received 2 Jan 2008; revised 14 Feb 2008; accepted 16 Feb 2008; published 20 Feb 2008

Using the estimated values of α, C, n = 5, and measured T_c's, we can calculate the best achievable energy resolution. Finally, taking into account that only ~ 0.4 fraction of the initial photoelectron energy is captured by the tungsten electron system [8], the expected resolution using Eq. (1) is 0.18 eV.

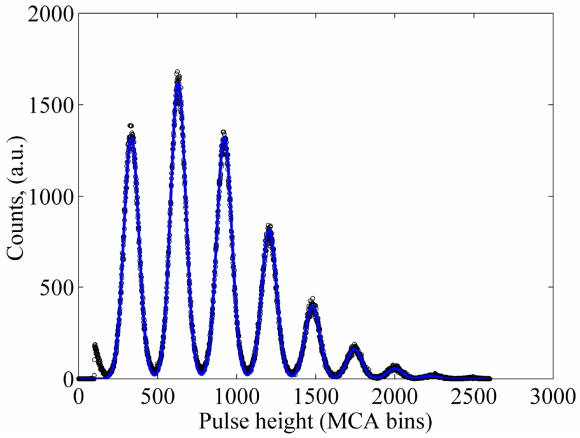

Fig. 5. (Color online) Pulse-height distribution of a pulsed laser source measured with the TES embedded in the optical cavity. The source was 80 ns wide pulses of 1556 nm laser light at a repetition rate of 50 kHz, with a mean photon number per pulse of μ ~ 2.45. Shown are the data (circles) and the fit (line) Poissonian distribution convolved with the energy resolution of the TES.

Figure 5 illustrates the pulse-height distribution from our TES photon counter in response to the 1556 nm (E=0.80 eV) laser, attenuated to give an average of ~ 2.463 photons per pulse. As Fig. 5 shows, the TES displays excellent discrimination between multiphoton events, up to 7 photons per pulse. In this measurement we used a pulsed 1556 nm laser with 80 ns pulse width and a repetition rate of 50 kHz. The solid line in Fig. 5 is the result of a fit of the data to a Poisson distribution for the number of photons detected convolved with the energy resolution of the device (a Gaussian function with standard deviation σ_E). For our pulsed laser, we expect the probability of producing an n-photon state as given by the Poisson distribution $P(n) = (\mu^n/n!)e^{-\mu}$, where $\mu = < n >$ is the mean number of photons per pulse. For our measurement, we expect the data to show this Poisson distribution, but with the mean number of absorbed photons per pulse reduced by multiplying by the system efficiency. A multi-peak fit to the data gives a value of μ = 2.449±0.002 (statistical error) for the average photon number and σ_E = 0.29 eV as the measured energy resolution (as the full width half maximum (FWHM) of histograms of pulse heights). The difference between the expected energy resolution and the measured resolution is due to noise from our electronics and possibly excess noise in the sensors [15].

Typical unfiltered pulses for zero-, one-, two-, three-, and four-photon events are displayed in Fig. 6. These sensors have thermal recovery times as short as 800 ns, which is significantly faster than the previous generation of optimized TES devices for absorption of 1550 nm light, which had decay times of 5 μs [10]. The faster recovery times are due to higher superconducting transition temperatures for the new generation TESs.

#91219 - $15.00 USD Received 2 Jan 2008; revised 14 Feb 2008; accepted 16 Feb 2008; published 20 Feb 2008

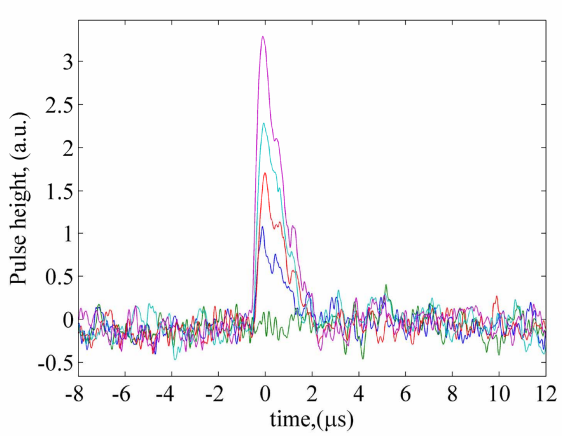

Fig. 6. (Color online) Detector response to 1556 nm (0.8 eV) photons. The pulses correspond to zero-, one-, two-, three-, and four-photon events, from the smallest height to the largest height traces. The measured (1/e) decay time is ~ 800 ns.

4.4 System detection efficiency at 1556 nm

The device detection efficiency is the ratio of the number of photons detected/counted by the TES to the number of the photons incident on the TES. To calculate the incident photon flux we must accurately determine the power incident on the device, which is not a trivial task because of the femtowatt power levels and the introduction of unknown losses through fiber components. Because commercial power meters lack the sensitivity required to measure such low power levels, our solution is to measure the milliwatt-level output power from a 1556 nm laser source and follow this laser with a series of three programmable optical attenuators [10]. Each attenuator is calibrated for attenuations between ~1 dB and ~ 40 dB for a tunable calibrated total attenuation between 3 dB and 120 dB. This technique enables accurate estimation of the number of photons in the optical fiber.

To accurately count the absorbed photon rate and reduce the sensitivity of our photon counting to background light, we used a pulsed laser source and a gated, multichannel analyzer (MCA) to record a histogram of the number of photons detected from each laser pulse. The MCA is gated to accept triggers only during a small time window (~100 ns) synchronous with the short (80 ns) laser pulse. Stray background light in the fiber due to blackbody radiation from room-temperature surfaces [16] is asynchronous and, therefore, these counts are reduced by a factor of 200 (given by the product of the gate interval and the 50 kHz repetition frequency of the laser).

The device efficiency can be determined by measuring the photon number statistics from the histogram of pulse heights and comparing this distribution to the expected Poisson distribution for the measured source power. However, it is relatively time consuming and difficult to minimize the statistical and systematic errors. Alternatively, instead of fitting to the photon number distribution to determine the mean photons per pulse detected, we can use the number of times the detector did *not* detect a photon to estimate the fraction of time $f(n = 0)$ we observed no photons. Assuming a Poisson distribution to the photon number, $f(n = 0)$ will be equal to $P(n = 0) = e^{-\mu}$, and therefore, the average number of photons detected per pulse is given by $-\ln f(n = 0)$.

Using this method of counting the number of times we did not see photons, we have measured 95 % system detection efficiency with a 2 % standard deviation over 40 measurements at various detector bias points and four different laser power levels for each bias point. The measured 95 % system detection efficiency is consistent with measurements and simulations of the optical elements and system losses. From Fig. 1., we estimate that the total absorption of the device is ~ 98 %. Coupling losses for fiber connectors and fiber

#91219 - $15.00 USD Received 2 Jan 2008; revised 14 Feb 2008; accepted 16 Feb 2008; published 20 Feb 2008

splices (our final measurement setup has three fiber splices and one fiber connector) can easily account for the ~ 2 % loss that we measure for the system detection efficiency when compared to the intrinsic detector efficiency. This result is quite promising for our efforts towards achieving a near-infrared photon-number resolving detector with > 99 % system detection efficiency with improvements in the multilayer design and reduction in connector and splicing loss.

5. Conclusion

We have fabricated near-unity efficiency, photon-number-resolving detectors optimized for absorption at 1550 and 1310 nm wavelengths. Using these detectors, we have measured a system detection efficiency of 95 % ± 2 % at 1556 nm, which to our knowledge is the highest system detection efficiency reported using a near-infrared single-photon detector. Because the measured absorption of the device structure is very close to the measured system efficiency, we are confident that we can increase beyond 95 % by fabricating the optical structure with tighter control over layer thicknesses, a higher reflectance mirror at the wavelengths of interest, and self-aligning schemes for eliminating the residual fiber-to-detector coupling losses.

Acknowledgments

The authors thank Alan Migdall, Tracy Clement, Eric Gansen for valuable technical discussions. The authors also thank IARPA and NIST Quantum Information Initiative for financial support.

#91219 - $15.00 USD Received 2 Jan 2008; revised 14 Feb 2008; accepted 16 Feb 2008; published 20 Feb 2008